Available online at www.sciencedirect.com
ScienceDirect
Catalysis Today 117 (2006) 220–227
CATALYSIS TODAY
www.elsevier.com/locate/cattod

CO oxidation catalyzed by gold nanoparticles confined in mesoporous aluminosilicate Al-SBA-15: Pretreatment methods

Chia-Wen Chiang, Aiqin Wang, Chung-Yuan Mou *

Center for Condensed Matter Sciences and Department of Chemistry, National Taiwan University, Taipei 106, Taiwan

Available online 27 June 2006

Abstract

Gold nanoparticles with an average size of ~3 nm confined in the mesoporous aluminosilicates Al-SBA-15 were synthesized by a procedure of successive aminosilane grafting and gold adsorption–reduction. The aluminosilicate, while traditionally regarded as an inert support for gold nanoparticles giving low activity for CO oxidation, was activated by a high-temperature hydrogen reduction pretreatment process and showed good catalytic activities in CO oxidation. We have made two different kinds of SBA-15, one templated by pluronic 123 with the normal method of synthesis (denoted as Al-SBA-15(N)) and the other templated by a ternary mixture of P123-CTAB-SDS (denoted as Al-SBA-15(F)) giving film morphology. It turns out the two support, although both can strongly confine the Au nanoparticles (NP) to ~3 nm, require different ways of pretreatments. Al-SBA-15(N) needs first calcination and then hydrogen reduction, but Al-SBA-15(F) needs a direct hydrogen reduction to give good catalytic activity. Electron paramagnetic resonance (EPR) measurements were performed for the catalyst at various stages of their treatments to identify the superoxide anion formation. The high-temperature hydrogen reduction of the aluminosilicate materials produces defect sites for oxygen adsorption to give the superoxide species which facilitates the CO oxidation.

Keywords: Gold; Catalysis; Nanoparticle; SBA-15; CO oxidation; Pretreatment; Support

1. Introduction

Gold catalyst in highly dispersed state has been proven very effective in many oxidation reactions [1], especially for low-temperature CO oxidation [2,3]. There are many factors affecting its catalytic activity; e.g. the size of gold nanoparticles [4–7], preparation methods [8–10], and pretreatment conditions [11–14]. However, they are often inter-related depending on choice of the support [15–17]. The most important factor in catalytic activity is the particle size of gold of which 3 nm is the optimum for CO oxidation. Various methods of controlling the particle size have been developed. Among these, we have recently prepared Au nanoparticles embedded within mesoporous aluminosilicates and used as catalysts for CO oxidation [18]. The functionalized mesoporous silica was used to absorb the gold precursor $AuCl_4^-$ and gold nanoparticles were formed inside the nanochannels after chemical reduction. The strong confinement of the nanopores of the mesoporous silica SBA-15 resulted in a very uniform size distribution of gold NP at ~3 nm [19]. However, traditionally aluminosilicate is considered to be an ''inert'' support giving poor catalytic activity for gold nanoparticle (NP) [17]. The nature of support affects both the activation of the oxygen and the size of the dispersed Au nanoparticles. The poor activity in gold NP supported on ''inert'' (including aluminosilicate) was generally considered as due to sintering and growing to large particle size of the gold NP [20]. This is because SiO_2 is known to have a relatively weak metal–support interaction with gold. Without proper confinement under high-temperature pretreatment, the gold NP would then grow to too large a size to have good catalytic activity. In our recent work, the gold nanoparticles confined in Al-SBA-15 are of the optimum size for catalysis of CO oxidation after high-temperature treatment. The problem of excessive sintering of gold nanoparticles is overcome by confining them in nanopores [19].

Once the size of gold nanoparticle is well controlled, then oxygen adsorption and activation on the catalyst is the crucial problem. Generally, some pretreatment procedure is necessary for activating the catalyst which depends on the support. It has been found that for reducible support such as Fe_2O_3, the

* Corresponding author. Fax: +886 2 2366 0954.
E-mail address: cymou@ntu.edu.tw (C.-Y. Mou).

0920-5861/$ – see front matter
doi:10.1016/j.cattod.2006.05.026

catalyst is active even without any high-temperature treatment [21]. For moderately reducible support such as TiO_2 or Al_2O_3, hydrogen reduction at a moderately high temperature is effective [22]. For example, in Yeh's work [22] the temperatures of hydrogen reduction are 373 and 473 K for Au/TiO_2 and Au/Al_2O_3, respectively. For acidic support, such as silica or aluminosilicate, past evaluation was based on the same relatively low-temperature pretreatment condition designed for TiO_2. Thus the general believe of poor activity in silica supported gold may be due to the less than optimum method of activation of the support. Bulushev et al. [23] recently found that for gold NP supported on activated carbon, a high-temperature reduction in H_2 (400–500 °C) was necessary to activate the catalyst. We found then that in our Au@Al-SBA-15 system, an even harsher condition for reduction was required [19]. An unusual high-temperature (600 °C) pretreatment in hydrogen was necessary for a good catalytic activity in CO oxidation. However, the cause and effect of the pretreatment process were not understood.

In this paper, we would like to compare the process of high-temperature treatment, calcination and reduction, between different mesoporous aluminosilicate supports. We would like to compare the two different kinds of Al-SBA-15 as supports. Although, they possess similar pore size and structure but we will show they need quite different methods of catalyst pretreatment. In our previous work, we have used a special kind of mesoporous Al-SBA-15(F) which was prepared from the ternary surfactant system CTAB-SDS-P123 and the resulting morphology is in thin film type [24]. Secondly, the silane APTS ($H_2N(CH_2)_3$–$Si(OMe)_3$) was used to surface-functionalize mesoporous silica [25]. In this work, we also use another thio-functional silane MPTS ($HS(CH_2)_3$–$Si(OMe)_3$) for surface functionalization. We then report on the catalytic activities of CO oxidation for these catalysts. Especial attention is paid to the catalysis under various pretreatment conditions. We then measure the electron paramagnetic resonance (EPR) of these catalysts and correlate with the catalytic activities. Finally, we discuss the activation process in the pretreatment.

The aluminosilicate support we choose to work on is traditionally regarded as very ''inert'' because it is not only non-reducible but also acidic. However, many applications of the catalysis are operated in an acidic environment. For example, in PROX fuel cell system where CO removal from hydrogen fuel is necessary, the proton transport-electrode media is rather acidic. If a CO catalyst system on acidic support can be much improved in the future, there will be great benefits.

2. Experimental section

2.1. Preparation of the catalyst

2.1.1. To synthesize the mesoporous aluminosilicate supports

In this paper, we use two different mesoporous aluminosilicates with the same Al amount; the thin film form and the normal form (Al-SBA-15(F) and Al-SBA-15(N)) as the catalyst supports. There is a similarity in the preparation method between the two supports, and they are both nano-sized and the Si/Al ratios of them are ca. 32 (determined by ICP).

The film type Al-SBA-15(F) was synthesized following our reported procedure [19]. A 0.7 g of triblock copolymer pluronic P123 and a proper amount of sodium aluminate were dissolved in 25 g of water, with the pH value adjusted to neutral, and followed by the addition of a surfactant mixture solution including 0.75 g of cetyltrimethylammonium bromide (CTAB) and 1.00 g of sodium dodecyl sulfate (SDS). Then the sodium silicate solution, with the pH value adjusted to 5–6, was added. The reaction proceeded at 40–50 °C for a certain amount of time. The resulting precipitate was filtered and collected. Another support, the normal kind (Al-SBA-15(N)), was synthesized by the similar method without the addition of the surfactant mixture solution (CTAB and SDS) and we also obtained the precipitates.

2.1.2. To prepare surface-modified mesoporous silica

A direct method of surface silyl modification and simultaneous surfactant removal of mesoporous silica was employed to obtain a silane loading of about 2–3 mmol/g of SiO_2 [13]. This direct method is known to lead to high and uniform surface loadings of silanes. A proper amount of mesoporous support was immersed in an ethanol solution of the silane APTS ($H_2N(CH_2)_3$–$Si(OCH_3)_3$) or MPTS ($HS(CH_2)_3$–$Si(OCH_3)_3$) and refluxed for 12–24 h at 80–90 °C. The products were recovered by filtration, washed with ethanol, and dried. The surfactants were also extracted during the same procedure.

2.1.3. To prepare the Au-containing mesoporous silica

A gold loading of 15–20 wt.% was achieved by adding 20 mL of a 25.4 mM aqueous $HAuCl_4$ solution to 1 g of the functionalized mesoporous support. The mixture was continuously stirred for 30 min. Then, the solid was filtered and dried in ambient conditions. Reduction of Au(III) was performed by adding 10 mL of a 0.1 M $NaBH_4$ aqueous solution to 0.5 g of the composite. After filtering and drying, the as-synthesized solid was obtained.

2.2. Catalysis tests

Before catalysis tests, the as-synthesized (without calcinations) catalyst was pretreated by heating to 600 °C under 10% H_2/N_2 flow and holding for 1 h, and then was cooled to room temperature under N_2 flow.

The catalysis test was run in a similar manner as previously reported [19]. The catalytic measurements were carried out in a packed bed within a quartz-tubular reactor (7 mm i.d.) under atmospheric pressure. A reaction gas containing 1% CO in air was passed over 20 mg of catalyst (after pretreatment) with a flow rate of 33 mL/min. The water vapor content in the reactant stream was no more than 4 ppm. The composition in the reactor out-stream was analyzed by using a Shimadzu GC-8A gas chromatography. This hydrogen reduction step at high temperature turns out to be crucial for good catalytic activity.

2.3. Characterization techniques

The powder X-ray diffraction patterns (XRD) were measured on a Scintag X1 reflection diffractometer operating with Cu Kα radiation. N_2 adsorption–desorption isotherms were performed at 77 K on a Micromeritics ASAP 2010 instrument, and the pore size distribution was calculated from the nitrogen adsorption isotherm using the Barrett–Joyner–Halenda (BJH) method. The electron microscopy images of Au nanoparticles were recorded on a JEOL JEM-2010 operated at 200 keV, and a mean size of the Au nanoparticles was estimated from the TEM images. Al and Au contents of the sample were analyzed with a simultaneous ICP–AES allied analytical system (Perking Elmer 3100 XL).

A Brüker EMX EPR spectrometer (X-band) was employed to measure the electron paramagnetic resonance (EPR) spectra of the samples. The powder sample used for the analysis was introduced in a quartz tubing of 4 mm outside diameter. The sample was sealed under vacuum. The spectrometer was equipped with a variable temperature controller, which allowed us to record spectra at low temperatures. Typical spectrometer settings were at a microwave frequency of 9.5 GHz, microwave power of 1.99 mW, and modulation amplitude of 12 G.

3. Results

3.1. Structural characterization of the catalyst

We first report the textural properties of the two catalyst supports, Al-SBA-15(F) and Al-SBA-15(N). For the purpose of comparison, their Al contents are fixed at the same Si/Al = 32. The porous nature of the products were confirmed by XRD and nitrogen adsorption–desorption isotherms (graphs not shown). Typical XRD and N_2 adsorption–desorption isotherms are similar to those of pristine SBA-15. In Table 1, we list the data of textural characterization of calcined supports. The two samples, Al-SBA-15(F) and Al-SBA-15(N), show similar pore volume. The film type, Al-SBA-15(F), gives a smaller pore size (4.6 nm) and a larger BET surface area.

Table 1
Characterization results of calcined Al-SBA-15(F) and Al-SBA-15(N) support

Calcined support	Si/Al[a]	d_{100}[b] (nm)	S_{BET} ($m^2\ g^{-1}$)	D_{pore} (nm)	V[c] ($cm^3\ g^{-1}$)
Al-SBA-15(F)	32	10.10	634	4.6	0.54
Al-SBA-15(N)	32	9.63	540	5.9	0.49

[a] The Si/Al molar ratios in products are determined by ICP.
[b] d_{100} calculated from Bragg equation: $2d \sin\theta = n\lambda$ ($\lambda = 0.1326$ nm).
[c] N_2 adsorption volume at $P/P_0 = 0.9$.

After loading of the gold NP, we analyzed its gold content. For most of the experiments, the loadings of Au are kept at about the same level at ∼17%, as shown in Table 2. We measured carefully the particle sizes of the gold nanoparticles embedded in the supports; in as-synthesized sample, and after calcination and hydrogen reduction or just simple reduction. The particle sizes for the as-synthesized catalyst (before any high-temperature treatment) are rather small, less than 2 nm. This proves that the strong confinement effect of the nanochannels of the Al-SBA-15. After hydrogen reduction at the high temperature of 600 °C, the particles grow a little. They are still mostly well confined within the nanopores with particles size between 2.6 and 3.2 nm (Table 2). It was observed that Al on the framework of Al-SBA-15 [19] not only generates surface acidity, but also limits the particle sizes of Au. Probably, the Al sites provide defect positions for anchoring Au nanoparticles, which may be helpful for the stabilization of gold nanoparticles. After calcination and hydrogen reduction, the particles grow a little bigger (5.1 and 3.2 nm for APTS and MPTS functionalized Al-SBA-15); but they are still confined in the nanochannels.

Fig. 1 shows the TEM micrographs for all the samples in Table 3. The upper row is for the APTS-functionalized system and lower row is for MPTS system. Fig. 1(a), (b), (f) and (g) in the left hand side are for film support sample, Au@APTS-Al-SBA-15(F). The rest in the right hand side are for Au@APTS-Al-SBA-15(N). We observe that in Fig. 1(a) the as-synthesized Au nanoparticles in APTS-Al-SBA-15(F) are rather small in size, about 1.6 nm, and it grows to 3.0 nm after hydrogen reduction treatment. In a separate experiment, when we used silica gel as support, the Au nanoparticle grows to well above 10 nm after similar treatment (figure not shown). The strong confinement effect of SBA-15 leads to a particle size less than its pore size. For MPTS-functionalized Al-SBA-15(F), the as-synthesized sample (Fig. 1(f)) gives somewhat non-uniform distribution of sizes. The smaller size is around 1 nm, but there are many particle of size around 3 nm. After H_2-reduction, the average diameter of Au NP is also 3.0 nm. We also observe Fig. 1(a) and (f), the nanochannels are parallel to the film plan, when Al is incorporated at Si/Al = 32. It seems at the high aluminum content, the channels are not vertical. For the normal kind of Al-SBA-15(N), the channels

Table 2
Characterization results of Au@silane-support catalyst with different support and grafting silane

Catalyst	Support	Grafting silane	Au loading[a] (wt.%)	Au size[b] (nm)		
				As-synthesized	H_2 reduction	Calcination and then H_2 reduction
a	Al-SBA-15(F)	APTS	17.97	1.6 ± 0.4	3.0 ± 0.8	5.1 ± 0.6
b	Al-SBA-15(N)	APTS	17.73	1.8 ± 0.4	3.2 ± 0.7	5.1 ± 1.0
c	Al-SBA-15(F)	MPTS	17.61	1.8 ± 0.9	3.0 ± 1.0	–
d	Al-SBA-15(N)	MPTS	17.07	1.0 ± 0.3	2.6 ± 0.4	3.2 ± 0.5

[a] Au loading detected by ICP–AES.
[b] Measured by TEM.

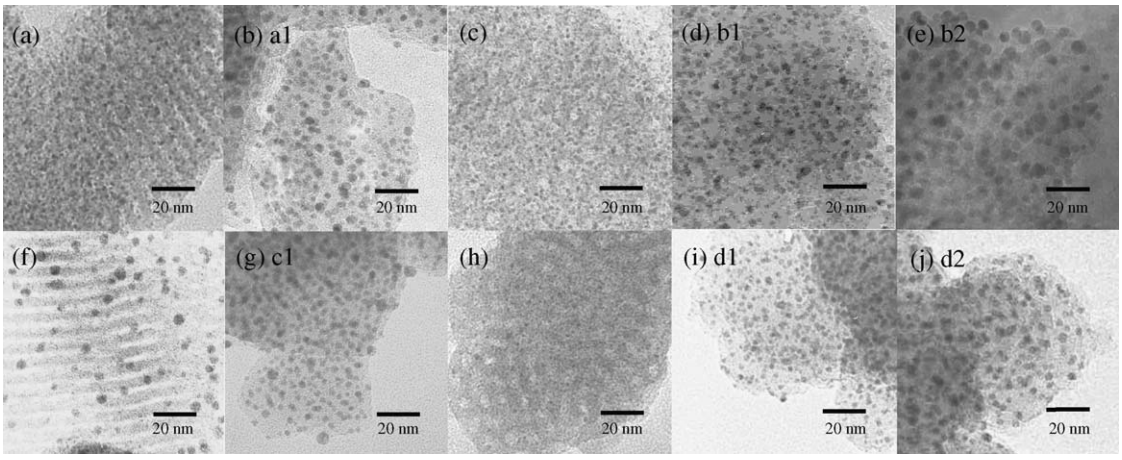

Fig. 1. TEM images of Au@APTS-Al-SBA-15(F) (catalyst a): (a) as-synthesized; (b) after H_2 reduction, Au@APTS-Al-SBA-15(N) (catalyst b); (c) as-synthesized; (d) after H_2 reduction; (e) after calcination and then H_2 reduction, Au@MPTS-Al-SBA-15(F) (catalyst c); (f) as-synthesized; (g) after H_2 reduction, and Au@APTS-Al-SBA-15(N) (catalyst d); (h) as-synthesized; (i) after H_2 reduction; (j) after calcination and then H_2 reduction.

Table 3
Pretreatment conditions (1 and 2) and catalytic performance of CO oxidation at 80 °C for Au@silane-support catalyst

Catalyst	Pretreatment conditions[a]		Au size[b] (nm)	Catalytic performance		
	Calcination	Reduction		Conversion[c] (%)	Reaction rate ($mol_{co}\ g_{cat}^{-1}\ s^{-1}$)	TOF[d] (s^{-1})
a1	No	Yes	3.0 ± 0.8	82.4	9.3×10^{-6}	2.5×10^{-2}
a2	Yes	Yes	5.1 ± 0.6	41.2	4.6×10^{-6}	2.0×10^{-2}
b1	No	Yes	3.2 ± 0.7	3.6	4.1×10^{-7}	1.1×10^{-3}
b2	Yes	Yes	5.1 ± 1.0	24.6	2.8×10^{-6}	1.2×10^{-2}
c1	No	Yes	3.0 ± 1.0	67.3	7.6×10^{-6}	2.1×10^{-2}
d1	No	Yes	2.6 ± 0.4	0.6	7.6×10^{-8}	1.8×10^{-4}
d2	Yes	Yes	3.2 ± 0.5	89.3	1.0×10^{-5}	2.9×10^{-2}

[a] Pretreatment was done before catalysis test. Two pretreatment conditions—1: reduction with N_2/H_2 and 2: calcination at 560 °C for 6 h and then reduction.
[b] Measured by TEM.
[c] The conversion value was took after 180 min reaction time.
[d] TOFs were calculated according to the relationship between the degree of dispersion and particle size as proposed by Bond and Thompson.

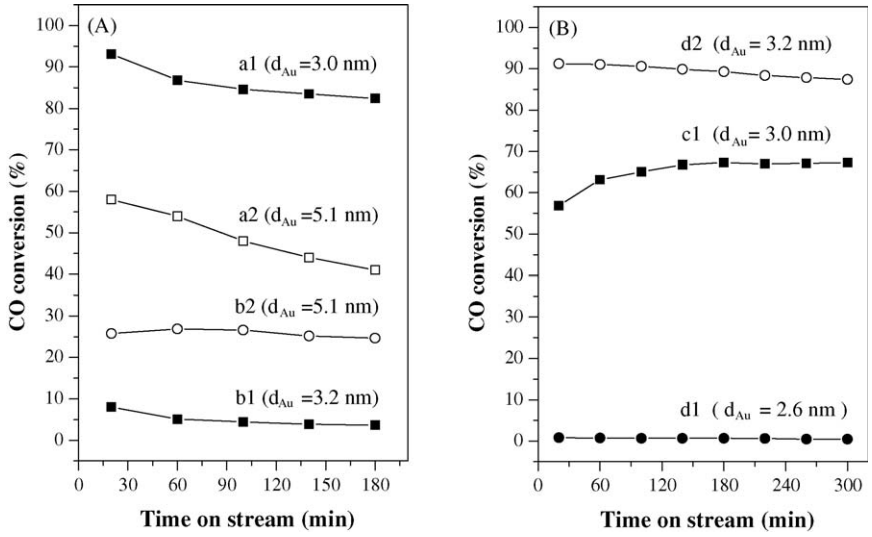

Fig. 2. Catalytic performance at 80 °C of (A) Au@APTS-Al-SBA-15(F) after H_2-reduction (sample a1), and after calcination and then H_2-reduction(sample a2); Au@APTS-Al-SBA-15(N) after H_2-reduction (sample b1),and after calcination and then reduction (sample b2); (B) Au@MPTS-Al-SBA-15(F) after H_2-reduction (sample c1), Au@MPTS-Al-SBA-15(N) after H_2-reduction (sample d1),and after calcination and then reduction (sample d2).

are somewhat disordered wormlike but the pore sizes are well defined. The loadings of gold are all very high as the high density of Au NP can be seen.

3.2. Catalytic activities

In Fig. 2, we report the catalytic conversion of CO at 80 °C for the catalysts made from APTS (Fig. 2(A)) and MPTS (Fig. 2(B)). We also compare between the film kind of SBA-15(F) and the normal kind of SBA-15(N). The first striking difference between the two supports is that for the film kind of SBA-15(F) support, hydrogen reduction is necessary to activate both catalysts, Au@APTS-Al-SBA-15(F) and Au@MPTS-Al-SBA-15(F). The curves a1 (for APTS) and c1 (for MPTS), representing Au supported on Al-SBA-15(F) after only hydrogen reduction, give high and steady conversion of CO. If one only calcined the catalyst, without the reduction process, the activity is nearly zero (plot not shown). If one does calcination and then reduction on SBA-15(F), the activity (a2 in Fig. 2) is a little lower than a1 (with reduction only). This may be due to the larger Au size (5.1 nm) of the a2 sample. However, for normal kind of support Al-SBA-15(N) good activation has to be calcination and then reduction (b2 and d2). If one only does the reduction for Al-SBA-15(N) without calcination, the activity is also pretty low (b1 and d1). Although the two kinds of support Al-SBA-15(F) and Al-SBA-15(N) look pretty similar in pore size and textural properties, they need quite different activation pretreatments to obtain good catalytic activity.

In Table 3, we list the steady state catalytic performance of CO oxidation at 80 °C for Au@silane-support catalysts under various pretreatment conditions. These include CO conversion, reaction rate and turnover frequency (TOF). TOFs are calculated from particle sizes of gold NP when they are measured.

Two pretreatment conditions are considered: (1) reduction with N_2/H_2 at 600 °C and (2) calcinations at 560 °C for 6 h and then reduction. The labels a–d for the catalysts mean the same as those in Table 2. Since their particle sizes are more or less the same due to the confinement of mesopores, the differences in catalytic activities are thus ascribed mostly to the pretreatment conditions. First, all the "good" catalyst require high-temperature hydrogen reduction before catalytic tests. For the film type Al-SBA-15(F), the catalyst directly reduced, without calcination, shows higher activity than the same materials with calcination and reduction (a1 versus a2 in Fig. 2). On the other hand, for Al-SBA-15(N) calcination is necessary; it needs calcination and then reduction to give best performance.

We have used rather high loading of Au (∼17%) in contrast to the usual ∼3%. We should point out that we deliberately designed our experiment this way to prove one of the main points in this work. What we want to show is that our use of mesoporous support can confined the Au nanoparticles so well even such a high loading of gold would not lead to uncontrolled growth of size above 3 nm after the high-temperature pretreatments (600 °C). Normally, with such a high loading of Au and high-temperature treatment on silica gel would have led to Au sizes above 10 nm (thus inactive). Anyway, we have reported the catalytic activities in TOF which is not dependent on loadings. However, we also need to examine the catalytic activities for lower loadings of Au. We prepared another two samples with 10% and 3% loadings of Au on SBA-15(F). Other pretreatment and reaction conditions are the same as a1 sample. The conversions of CO are shown in Fig. 3. As expected the activities are lower than that of a1 sample. However, we notice that the activities are disproportionally low with respect to the loadings. Upon closer examination of the average particle sizes by TEM, we found they are ∼2.3 nm—smaller than the optimum size of 3 nm. The lower loadings lead to lesser aggregation and the size of 2.3 nm is probably the cause of lesser catalytic activity because it is below the optimum size for catalysis. This shows that for the aluminosilicate supports the activity is rather size-sensitive for Au nanoparticles as we have previously reported [18].

3.3. Electron paramagnetic resonance

For better understanding the origin of the different catalytic behavior under various pretreatment processes, we study the electronic defects in the various samples by EPR technique. EPR is a highly sensitive technique to study electronic defects and redox process, especially when involving electron transfer species. In this work, EPR spectra were measured on catalysts on different supports with various pretreatments, so as to compare their differences in oxygen activation. Since catalysts made from APTS and MPTS functionalizations give similar results, we focus here only on the system Au@APTS-Al-SBA-

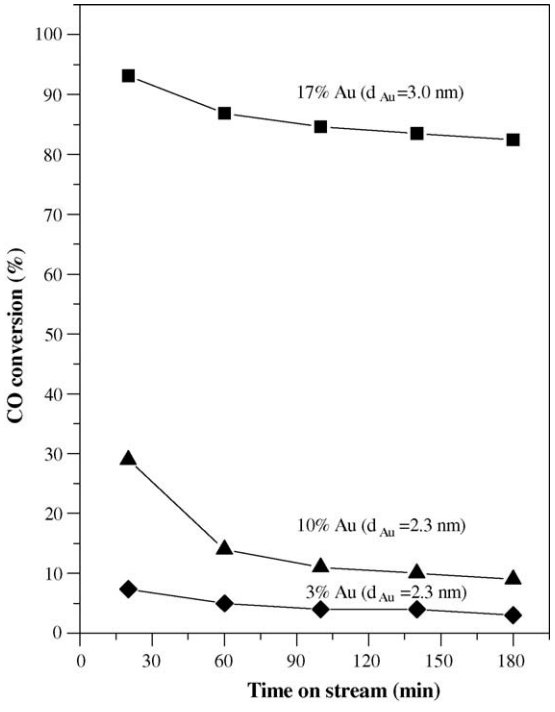

Fig. 3. Catalytic performance at 80 °C of Au@APTS-Al-SBA-15(F) at different Au loadings: (a) 17% Au (sample a1); (b) 10% Au; (c) 3% Au.

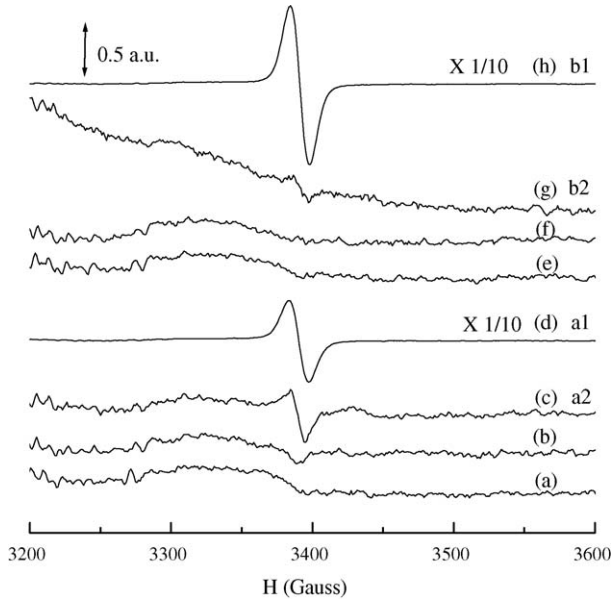

Fig. 4. EPR spectra of the catalyst at various stages of its synthesis. Au@APTS-Al-SBA-15(F): (a) as-synthesized; (b) after calcinations; (c) after calcinations and then reduction by hydrogen at 600 °C; (d) after reduction. Au@APTS-Al-SBA-15(N); (e) as-synthesized; (f) after calcinations; (g) after calcinations and then reduction by hydrogen at 600 °C; (h) after reduction.

15. From Okumura's work [26] and our previous study [27], the main EPR signal at $g = 2.009$ is assigned to the superoxide O_2^- formed on the catalyst surface. The EPR intensities of O_2^- are measured and illustrated in Fig. 4. We found that both as-synthesized (Fig. 4(a) and (e)) and after-calcination sample (Fig. 4(b) and (f)) gave weak and featureless EPR spectra. There is very little formation of superoxides. This correlates well with the finding that catalytic activities for these samples are nearly zero. Apparently, the calcinations step by itself is not enough for activating the catalysts. The weak broad bands at 3300–3400 G are probably due to various electronic defects in the sample.

With hydrogen reduction treatment, the intensity of O_2^- increased greatly (a1 and b1 in Fig. 4). For all the samples, we did not observe the anisotropic EPR signal expected of localized superoxide radical anions [28]. Instead, we always observed a single broadened EPR signal, implicating a rather mobile superoxide species. The film sample a1, obtained from direct reduction without calcination, produces a much stronger superoxide signal (Fig. 4, curve d). With calcination and reduction, the superoxide signal is weaker. This roughly reflects the difference in catalytic activities between samples a1 and a2. Apparently, in the catalyst system Al-SBA-15(F), the oxidation process is limited by the oxygen supply and the activation through superoxide formation is rate-determining.

Surprisingly, the normal Al-SBA-15(N) support gives quite a different behavior in EPR spectra. The direct reduction process gives the strongest EPR intensity (for b1), but the b1 sample gives a fairly low catalytic activity. On the other hand the b2 sample, which was treated with calcination and reduction and gave high activity, while producing a relatively low intensity of the superoxide. For b2, a pretty broad and strong EPR band was obtained (Fig. 4, curve g), reflecting very complicated electronic defect structures. This behavior needs further study in the future.

4. Discussions

We have shown in this report a method of surface functionalization of mesoporous silica with amine or thio-functional silane which can give high loadings of gold precursors. Reduction and high-temperature pretreatment produce Au NP of ~3 nm size, the optimum size for catalytic activity. Uncontrolled growth, under high-temperature pre-treatment, of gold nanoparticles is limited by pore confinement. Moderately strong catalytic activities for CO oxidation are found for the Au@SBA-15 system; the TOF is better than those reported on Au supported on silica (Table 3) [29,30]. Part of the reason of our success is due to the strong pore confinement leading to optimum particle sizes of Au NP. Otherwise, the weak metal–support interaction between gold and silica would easily lead to particle aggregation and growth to large inactive Au NP. Although our loadings of Au near 17% is a lot higher than the usual ~3% for Au support on active metal oxides in most of the reported work, we were still able to obtain very small Au particles (~3 nm). In fact, when using silica gel as supports, such a high loading of Au would have led to Au NP particle size much bigger than 5 nm and thus to an inactive catalyst. Since TOFs are calculated based on per mol surface Au atom, the good catalytic activities reflect good surface reaction rate of CO oxidation on Au NP. Previously, Haruta and coworkers [16], using chemical vapor deposition (CVD) method, were able to confine Au NP within the nanochannels of MCM-41 materials and found a surprisingly active catalyst for CO oxidation. Together with our results here, these indicate that good control of Au NP's size is rather crucial for inert support such as silica or aluminosilicates.

It seems the catalytic activities of CO oxidation of the two catalysts from aminosilane and thiosilane are comparable (compare a1 and c1 in Table 3 for example). This is because that the surface protecting ligands are completely removed by the high-temperature pretreatments and the catalytic activity depends mainly on the support and the surface defects on it.

For the support aluminosilicate, traditionally regarded as inert [17], the other important contribution in this paper is that we have found a pretreatment method to activate the catalyst. The high-temperature hydrogen reduction process leads to changes in the electronic defects in the support which we would like now to focus our attentions to. In general, the chemical and electronic properties of surfaces are mostly controlled by defects. For supported Au catalysts there is general agreement that CO is adsorbed on the gold particles, and that the CO oxidation reaction occurs on the surface of the catalyst with co-adsorbed oxygen [13,17]. However, the mechanism for oxygen adsorption and activation is not yet clear. Various surface sites for oxygen activation have been proposed; such as gold surface, defect site or metal/oxide peripheral of support oxide. Iwasawa and coworkers [8] suggested adsorption of molecular super-oxide oxygen species occurs on the support, possibly on oxygen

vacancies (F+ center), which should be available on semiconductor (reducible) materials such as TiO_2, Fe_3O_4, or ZnO. Recently, Andreeva and coworkers [31] has detected F-centers (at $g = 2.002$), an oxygen vacancy with an electron, in mesoporous titania and zirconia by EPR. Theoretical calculations have shown that F-centers on oxide surfaces can activate Au by transfer of electronic charge from the surface to the clusters [32]. Upon adsorption of oxygen, it is thus reasonable to expect the electron transfer from F-center to oxygen to produce superoxide radical anion. If the superoxide ion is mobile, it can supply the activated oxygen to react with CO on the Au NP. In fact, recently Filimonov and coworkers [28] have just performed an EPR study of ceria–silica catalyst and found localization of superoxide radical anion on the defect sites which were produced by hydrogen reduction. It is known CeO_2 easily produces defect sites, especially under hydrogen reduction. Goodman has concluded defects facilitate the adsorption of oxygen and also serve as sites for nucleation, growth, and stability of metal clusters on metal oxide surfaces [33,34].

From the above survey, we surmise that active supports are those metal oxide that can give electron-rich defects where electrons can be transferred to surface oxygen species in catalysis. For aluminosilicates, we have shown that this activation is possible only under harsh hydrogen reduction process in which the oxygen atom in Si–O–Si may be abstracted by hydrogen to produce the defect. This would produce an electron-rich defect, such as F-center, which may be the electron source for superoxide upon oxygen adsorption. It seems simple calcinations is not enough for the production of these kind of electron-rich defects. In many of the past works, where simple activation of catalyst by calcinations was employed, the supports were mostly the active kind, such as TiO_2. In active support such as TiO_2, MgO or Fe_3O_4, the defects either exist at room temperature or can be generated by simple calcination. The calcination serves the dual purpose of reducing $Au(OH)_3$ to give Au NP and activate the support. For example, in the case of TiO_2 support, Okumura et al. [26] found that CO adsorption at room temperature on freshly activated (calcined at 673 K) Au/TiO_2 can abstract oxygen ions from the support surface producing Ti^{3+} and oxygen vacancy site.

For inert supports, usually insulator with large band gap [17], it was argued that oxygen activation takes place on the surface of gold. The inert supports only play an indirect role in affecting the degree of dispersion of gold. However, in this paper we found that proper strong hydrogen treatment at high temperature can produce electron-rich defects to activate oxygen. In such case, calcination is oxidative and not so effective for the purpose. Indeed, from Fig. 4 we found that strong signals due to superoxides are produced for those samples under high-temperature reduction solely (a1 and b1). For the aluminosilicate Al-SBA-15, we have previously shown that Al content also helps the catalytic conversion in CO oxidation [19]. Probably, Al serves as a defect site upon hydrogen reduction. The role of Al in limiting the size of Au NP and the activation of oxygen is the subject of another report [35].

The optimum pretreatment methods and thus their defect structures in the two types Al-SBA-15 seem to be different. The main difference between the two supports seems to be the extra surfactants CTAB and SDS employed in the fabrication of Al-SBA-15(F). Although we believe the surfactants are mostly removed in the calcinations or high-temperature reduction process, the elements N (from CTAB) and S (from SDS) could be present in the support in trace amount and help the formation of defects different from those in Al-SBA-15(N). Since defects are very sensitive to minor components of impurity, this may not be very surprising. This will need further studies.

In this work, we have used a fairly high loading of gold (at ~17%). However, it turns out this high loading would just lead to a good average size of gold (~3 nm) giving good TOF numbers. For the ''inert'' aluminosilicate support, the catalysis is very much size-sensitive. For size smaller than 3 nm, the activity would be less than optimum. If one wants to use a lower loading of gold, then one may need to further prolong the high-temperature pretreatment to bring up the particle size to reach higher activity. Further fine-tuning in the preparation and pretreatment of the catalyst along this direction would be interesting.

We note finally the mesoporous materials we used as support, Al-SBA-15, is acidic in nature. Au nanocatalysts supported on acidic support are much less explored because of lack of suitable preparation method for them. Often too large of Au nanoparticles were obtained, thus leading to low activities. However, they are potentially important in PROX fuel cell system where CO removal from hydrogen fuel is necessary [36]. In this work, we have shown a method of precisely control the particle size and the activation of the catalyst. Further progress in this direction would be very useful.

Acknowledgement

This work was supported by a grant from the National Science Council through Academy Excellence program.

References

[1] M. Haruta, Catal. Today 36 (1997) 153.
[2] C.K. Costello, J.H. Yang, H.Y. Law, Y. Wang, J.N. Lin, L.D. Marks, M.C. Kung, H.H. Kung, Appl. Catal. A 243 (2003) 15.
[3] G.C. Bond, D.T. Thompson, Catal. Rev.-Sci. Eng. 41 (1999) 319.
[4] M. Valden, X. Lai, D.W. Goodman, Science 281 (1998) 1647.
[5] M. Haruta, Catal. Today 36 (1997) 153.
[6] W.T. Wallace, R.L. Whetten, J. Phys. Chem. B 104 (2000) 10964.
[7] D.C. Meier, D.W. Goodman, J. Am. Chem. Soc. 126 (2004) 1892.
[8] H. Liu, A.I. Kozlov, A.P. Kozlova, T. Shido, K. Asakura, Y. Iwasawa, J. Catal. 185 (1999) 252.
[9] A.I. Kozlov, A.P. Kozlova, K. Asakura, Y. Matsui, T. Kogure, T. Shido, Y. Iwasawa, J. Catal. 196 (2000) 56.
[10] A.A. Wolf, F. Schüth, Appl. Catal. A 226 (2002) 1.
[11] L. Guczi, D. Horváth, Z. Pászti, G. Petõ, Catal. Today 72 (2002) 101.
[12] W.F. Yan, B. Chen, S.M. Mahurin, V. Schwartz, D.R. Mullins, A.R. Lupini, S.J. Pennycook, S. Dai, S.H. Overbury, J. Phys. Chem. B 109 (2005) 10676.
[13] F. Boccuzzi, A. Chiorino, M. Manzoli, P. Lu, T. Akita, S. Ichikawa, M. Haruta, J. Catal. 202 (2001) 256.
[14] A.Q. Wang, C.M. Chang, C.Y. Mou, J. Phys. Chem. B 109 (2005) 18860.

[15] R.J.H. Grisel, B.E. Nieuwenhuys, J. Catal. 199 (2001) 48.
[16] M. Okumura, S. Nakamura, S. Tsubota, T. Nakamura, M. Azuma, M. Haruta, Catal. Lett. 51 (1998) 53.
[17] M.M. Schubert, S. Hackenberg, A.C. van Veen, M. Muhler, V. Plzak, R.J. Behm, J. Catal. 197 (2001) 113.
[18] Y.S. Chi, H.P. Lin, C.Y. Mou, Appl. Catal. A 284 (2005) 199.
[19] C.W. Chiang, A. Wang, B.Z. Wan, C.Y. Mou, J. Phys. Chem. B 109 (2005) 18042.
[20] W.T. Wallace, B.K. Min, D.W. Goodman, J. Mol. Catal. A 228 (2005) 3.
[21] S.T. Daniells, A.R. Overweg, J.M. Makkee, J.A. Moulijn, J. Catal. 230 (2005) 52.
[22] Y.J. Chen, C.T. Yeh, J. Catal. 200 (2001) 59.
[23] D.A. Bulushev, I. Yuranov, E.I. Suvorova, P.A. Buffat, L. Kiwi-Minsker, J. Catal. 224 (2004) 8.
[24] B.C. Chen, H.P. Lin, M.C. Chao, C.Y. Mou, C.Y. Tang, Adv. Mater. 18 (2004) 1687.
[25] Y.H. Liu, H.P. Lin, C.Y. Mou, Langmuir 20 (2004) 3231.
[26] M. Okumura, J.M. Coronado, J. Soria, M. Haruta, J.C. Conesa, J. Catal. 203 (2001) 168.
[27] A.Q. Wang, J.H. Liu, S.D. Lin, T.S. Lin, C.Y. Mou, J. Catal. 233 (2005) 186.
[28] A. Aboukais, E.A. Zhilinskaya, J.F. Lamonier, I.N. Filimonov, Colloids Surf. A 260 (2005) 199.
[29] A.M. Venezia, L.F. Liotta, G. Pantaleo, V. La Parola, G. Deganello, A. Beck, Z. Koppány, K. Frey, D. Horváth, L. Guczi, Appl. Catal. A 251 (2003) 359.
[30] M. Date, M. Okumura, S. Tsubota, M. Haruta, Angew. Chem. Int. Ed. 43 (2004) 2129.
[31] L. Ilieva, J.W. Sobczak, M. Manzoli, B.L. Su, D. Andreeva, Appl. Catal. A: Gen. 291 (2005) 85.
[32] N. Lopez, T.V.W. Janssens, B.S. Clausen, Y. Xu, M. Mavrikakis, T. Bligaard, J.K. Norskov, J. Catal. 223 (2004) 232.
[33] W.T. Wallace, B.K. Min, D.W. Goodman, J. Mol. Catal. A 228 (2005) 3.
[34] Z. Yan, S. Chinta, A.A. Mohamed, J.P. Fackler, D.W. Goodman, J. Am. Chem. Soc. 127 (2005) 1604.
[35] A.Q. Wang, Y.P. Hsieh, Y.F. Chen, C.Y. Mou, J. Catal. 237 (2005) 197.
[36] D. Cameron, R. Holliday, D. Thompson, J. Power Sources 118 (2003) 298.